Lawrence Berkeley National Laboratory

Title
Demonstration Report: ESTCP UXO Discrimination Study ESTCP PROJECT # MM-0838

Permalink
https://escholarship.org/uc/item/9cn4804g

Author
Gasperikova, Erika

Publication Date
2010-06-01

Peer reviewed

DEMONSTRATION REPORT

ESTCP UXO DISCRIMINATION STUDY
ESTCP PROJECT # MM-0838

SITE LOCATION:
FORMER CAMP SAN LUIS OBISPO, SAN LUIS OBISPO, CA

DEMONSTRATOR:
LAWRENCE BERKELEY NATIONAL LABORATORY
ONE CYCLOTRON ROAD, MS: 90R1116
BERKELEY, CA 94720
p.o.c. Erika Gasperikova, egasperikova@lbl.gov, 510-486-4930

TECHNOLOGY TYPE/PLATFORM:
BUD/CART

FEBRUARY 2010

TABLE OF CONTENTS

1. INTRODUCTION

1.1 Background

In 2003, the Defense Science Board observed: "The … problem is that instruments that can detect the buried UXOs also detect numerous scrap metal objects and other artifacts, which leads to an enormous amount of expensive digging. Typically 100 holes may be dug before a real UXO is unearthed! The Task Force assessment is that much of this wasteful digging can be eliminated by the use of more advanced technology instruments that exploit modern digital processing and advanced multi-mode sensors to achieve an improved level of discrimination of scrap from UXOs."

Significant progress has been made in discrimination technology. To date, testing of these approaches has been primarily limited to test sites with only limited application at live sites. Acceptance of discrimination technologies requires demonstration of system capabilities at real UXO sites under real world conditions. Any attempt to declare detected anomalies to be harmless and requiring no further investigation will require demonstration to regulators of not only individual technologies, but of an entire decision making process. This characterization study was be the second phase in what is expected to be a continuing effort that will span several years.

The FY06 Defense Appropriation contained funding for the "Development of Advanced, Sophisticated, Discrimination Technologies for UXO Cleanup" in the Environmental Security Technology Certification Program (ESTCP). ESTCP responded by conducting a UXO Discrimination Study at the former Camp Sibert, AL. The results of this first demonstration were very encouraging. Although conditions were favorable at this site, a single target of interest (4.2-in mortar) and benign topography and geology, all of the classification approaches demonstrated were able to correctly identify a sizable fraction of the anomalies as arising from non-hazardous items that could be safely left in the ground. To build upon the success of the first phase of this study, ESTCP sponsored a second study in 2009 at the former Camp San Luis Obispo, CA, a site with more challenging topography and a wider mix of targets-of-interest (TOI).

1.2 Objectives of the Demonstration

1.2.1 Objectives of the ESTCP UXO Discrimination Study

There were two primary objectives of this study:

(1) Test and validate detection and discrimination capabilities of currently available and emerging technologies on real sites under operational conditions.

(2) Investigate in cooperation with regulators and program managers how discrimination technologies can be implemented in cleanup operations.

1.2.2 ESTCP Technical objectives of the Discrimination Study

(1) Test and evaluate capabilities by demonstrating and evaluating individual sensor and discrimination technologies and processes that combine these technologies. Compare advanced methods to existing practices and validate the pilot technologies for the following:

    (a) Detection of UXOs

    (b) Identification of features that distinguish scrap and other clutter from UXO

    (c) Reduction of false alarms (items that could be safely left in the ground that are incorrectly classified as UXO) while maintaining Pds acceptable to all

    (d) Ability to identify sources of uncertainty in the discrimination process and to quantify their impact to support decision making, including issues such as impact of data quality due to how data is collected

    (e) Quantify the overall impact on risk arising from the ability to clear more land more quickly for the same investment.

    (f) Include the issues of a dig-no dig decision process and related QA/QC issues

(2) Understand the applicability and limitations of the pilot technologies in the context of project objectives, site characteristics, suspected ordnance contamination

(3) Collect high-quality, well-documented data to support the next generation of signal processing research.

1.2.3 LBNL Objective

The demonstration objective was to determine the discrimination capabilities of the Berkeley UXO Discriminator (BUD) at San Luis Obispo, CA. Lawrence Berkeley National Laboratory (LBNL) performed a cued mode discrimination survey. The data were collected in accordance with the overall study demonstration plan, including the system characterization with the emplaced calibration items along a calibration line and at a test pit.

1.3 Regulatory Drivers

ESTCP has assembled an Advisory Group to address the regulatory, programmatic and stakeholder acceptance issues associated with the implementation of discrimination in the munitions response process.

Objective of Advisory Group:

Help the ESTCP Program Office explore a UXO discrimination process that will be useful to regulators and managers in making decisions.

    (1) Under what conditions would you consider discrimination?

    (2) What does a pilot project need to demonstrate for the community to consider not digging every anomaly as a viable alternative?

        (a) Methodology

        (b) Transparency

        (c) QA/QC requirements

        (d) Validation

    (3) For implementation beyond the pilot project,

        (a) How should proposals to implement discrimination be evaluated?

        (b) Site suitability

            Geology

            Anomaly density

            Site topography

            Level of understanding of expected UXO types

        (c) Track record on like sites

        (d) Performance on test site or small subset of site

(e) Understanding and management of uncertainties

(4) Define data needs to support decisions, particularly with regard to decisions not to dig all detected anomalies

(5) Define acceptable end-products to support discrimination decisions.

In support of the above, provide input and guidance to the ESTCP Program Office:

o Pilot project objectives and flow-down to metrics

o Flow down of program objectives to data quality objectives

o Demonstration/Data collection plans

o QA/QC requirements and documentation

o Interpretation, Analysis, and Validation

o Process flow for discrimination-based removal actions

2. TECHNOLOGY DESCRIPTION

2.1 Technology Development and Application

The ESTCP has supported LBNL in the development of the Berkeley UXO Discriminator (BUD) that not only detects the object itself but also quantitatively determines its size, shape, and orientation. Furthermore, BUD performs target characterization from a single position of the sensor platform above a target. BUD was designed to detect UXO in the 20 mm to 155 mm size range for depths between 0 and 1.5 m, and to characterize them in a depth range from 0 to 1.1 m. The system incorporates three orthogonal transmitters, and eight pairs of differenced receivers. The transmitter-receiver assembly together with the acquisition box, as well as the battery power and global positioning system (GPS) receiver, is mounted on a small cart to assure system mobility. System positioning is provided by state-of-the-art Real Time Kinematic (RTK) GPS receiver. The survey data acquired by BUD are processed by software developed by LBNL, which is efficient and simple, and can be operated by relatively untrained personnel. BUD is shown in Figure 1.

Figure 1. Berkeley UXO Discriminator (BUD)

The BUD employs three orthogonal transmitters and eight pairs of differenced receivers. Eight receiver coils are placed horizontally along the two diagonals of the upper and lower planes of the two horizontal transmitter loops. These receiver coil pairs are located on symmetry lines through the center of the system and each pair sees identical fields during the on-time of current pulses in the transmitter coils. They are wired in opposition to produce zero output during the on–time of the pulses in three orthogonal transmitters. This configuration dramatically reduces noise in measurements by canceling background electromagnetic fields (these fields are uniform over the scale of the receiver array and are consequently nulled by the differencing operation), and by canceling noise contributed by the tilt of the receivers in the Earth's magnetic field, and greatly enhances receivers' sensitivity to gradients of the target response.

Data acquisition is performed on a single board. The transmitter coils are powered separately from the data acquisition board. Pulsers provide resonant circuit switching to create bi-polar half-sine pulses of 350 μs width. The current has a ~18 A peak and a resonant circuit voltage of ~750 Volts. The operational overall half-sine duty cycle is ~12%. The resonant frequency of the inductive load is ~90 kHz. Transients are digitized with a sampling interval of 4 μs. The sensors are critically damped 6-inch 325 turn loops with a self-resonant frequency of 25 kHz. The data acquisition board has 12 high-speed ADC channels for output. Eight of these channels are used for the signal from receiver coils, and the remaining four channels provide information about the system (i.e. tilt information, time stamps, transmitter current).

It has been demonstrated that a satisfactory classification scheme is one that determines the principal dipole polarizabilities of a target – a near intact UXO displays a single major polarizability coincident with the long axis of the object and two equal transverse polarizabilities. The induced moment of a target depends on the strength of the transmitted inducing field. The moment normalized by the inducing field is the polarizability. This description of the inherent polarizabilities of a target is a key in discriminating UXO from irregular scrap metal. Figures 2-4 illustrate a discrimination capability of the system for UXO objects (Figures 2 and 3), and a scrap metal (Figure 4). All three figures have estimated principal polarizabilities as a function of time plotted on the left, values of true and estimated location and orientation on the right, and object images at the bottom. While UXO objects have a single major polarizability coincident

with the long axis of the object and two equal transverse polarizabilities (Figure 2-3), the scrap metal exhibits three distinct principal polarizabilities (Figure 4). The locations and orientations are recovered within a few percent of true values for all three objects. Moreover, UXO have unique polarizability signatures, and thus distinctions can be made among various UXOs.
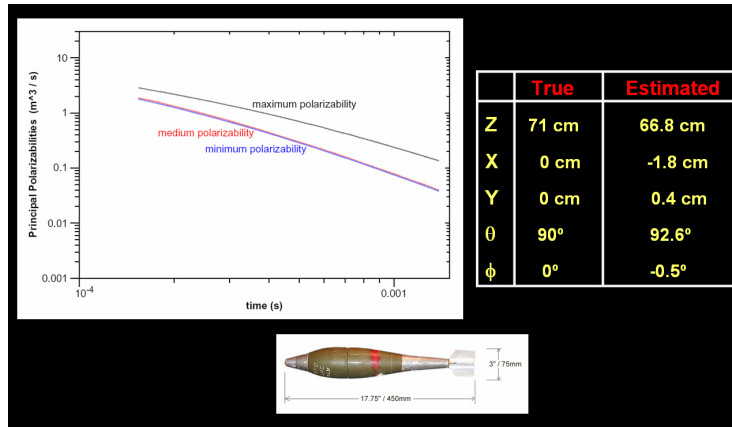

Figure 2. Inversion results for the principal polarizabilities, location and orientation of 81 mm M821A1 projectile
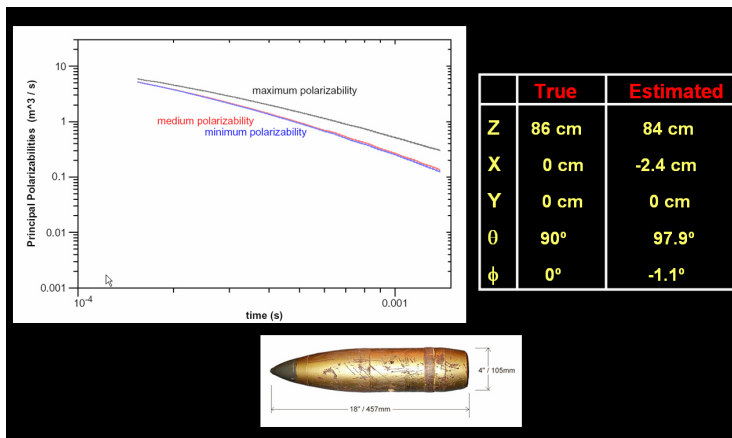

Figure 3. Inversion results for the principal polarizabilities, location and orientation of 105 mm M60 projectile
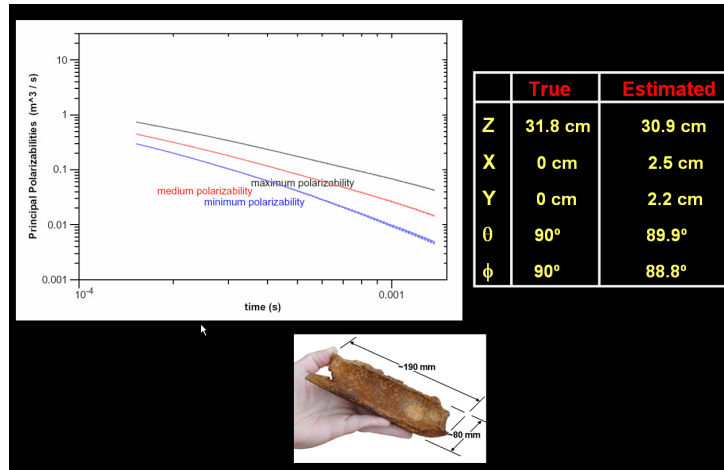
Figure 4. Inversion results for the principal polarizabilities, location and orientation of 19x8 cm scrap metal

The detection performance of the system is governed by an object's size-depth relationship. If we assume that BUD's lower receiver plane is 0.2 m above the ground, the system can detect and discriminate objects with depth uncertainty of 10% down to 1.3 m and 0.9 m, respectively. Any objects buried at the depth more than 1.3 m and 0.9 m will have a low probability of detection and discrimination, respectively.

Object orientation estimates and equivalent dipole polarizability estimates used for large and shallow UXO/scrap discrimination are more problematic as they are affected by higher order (non-dipole) terms induced in objects due to source field gradients along the length of the objects. For example, a vertical 0.4 m object directly below the system needs to be about 0.90 m deep for perturbations due to gradients along the length of the object to be of the order of 20 % of the uniform field object response. Similarly, vertical objects 0.5 m, and 0.6 m long need to be 1.15 m, and 1.42 m, respectively, below the system. For horizontal objects the effect of gradients across the objects' diameter are much smaller. For example, 155 mm and 105 mm projectiles need to be only 0.30 m, and 0.19 m, respectively, below the system. A polarizability index (in cm^3), which is an average value of the product of time (in seconds) and polarizability rate (in m^3/s) over the 35 sample times logarithmically spaced from 140 to 1400 μs, and three polarizabilities, can be calculated for any object. In this survey, we used this polarizability index to decide when the object is in a uniform source field. Objects with the polarizability index

smaller than 600 cm^3 and deeper than 1.8 m below BUD, or smaller than 200 cm^3 and deeper than 1.35 m, or smaller than 80 cm^3 and deeper than 0.90 m, or smaller than 9 cm^3 and deeper than 0.20 m below BUD are sufficiently deep that the effects of vertical source field gradients should be less than 15% and are not expected to be a problem. All other objects are considered large and shallow objects. For the object characterization, UXO/scrap discrimination, measurements at each flag were taken on a grid as shown in Figure 7. This allows the system get further away from the object, and hence minimizes source gradients, at one or more locations in the case that a large shallow object is found.

2.2 Previous Testing of the Technology

The performance of the BUD has been demonstrated at our local test site in California, as well as the Calibration and Blind Test Grids and the Open Field Range at the Yuma Proving Ground (YPG), AZ, Camp Sibert, AL, and FE Warren AFB, WY. The results have been presented at various meetings and published in scientific journals.

2.3 Advantages and Limitations of the Technology

This system not only detects but also discriminates UXO from non-UXO/scrap and gives its characteristics (location, size, polarizability, aspect ratio) from a single position of the sensor platform above the object. BUD was designed to detect and discriminate UXO in the 20 mm to 155 mm size range buried anywhere from 0 to 1.5 m depth and from 0 to1.1 m, respectively. Any objects buried at the depth more than 1.5 m will have a low probability of detection, and any objects buried at the depth more than 1.1 m will have a low probability of discrimination. With existing algorithms in the system computer it is not possible to recover the principal polarizabilities of large objects close to the system. Detection of large shallow objects is assured, but at present discrimination is not. Post processing of the field data is required for shape discrimination of large shallow targets. See Chapter 2.1 for details.

3. DEMONSTRATION DESIGN

3.1 Period of Operation

The BUD cued discrimination survey at San Luis Obispo took place between June 22, 2009 and July 9, 2009. Data were collected over 244 flags in the south grid and 295 flags in the east grid shown in yellow in Figure 5. The gray area in Figure 5 indicates the location of training data for our discrimination analysis. The ESTCP office provided the locations of these flags. Data acquisition took 13 working days. We had no down time with the system, and finished the survey ahead of schedule. The field crew consisted of three people, and the PI was present a part of the survey.
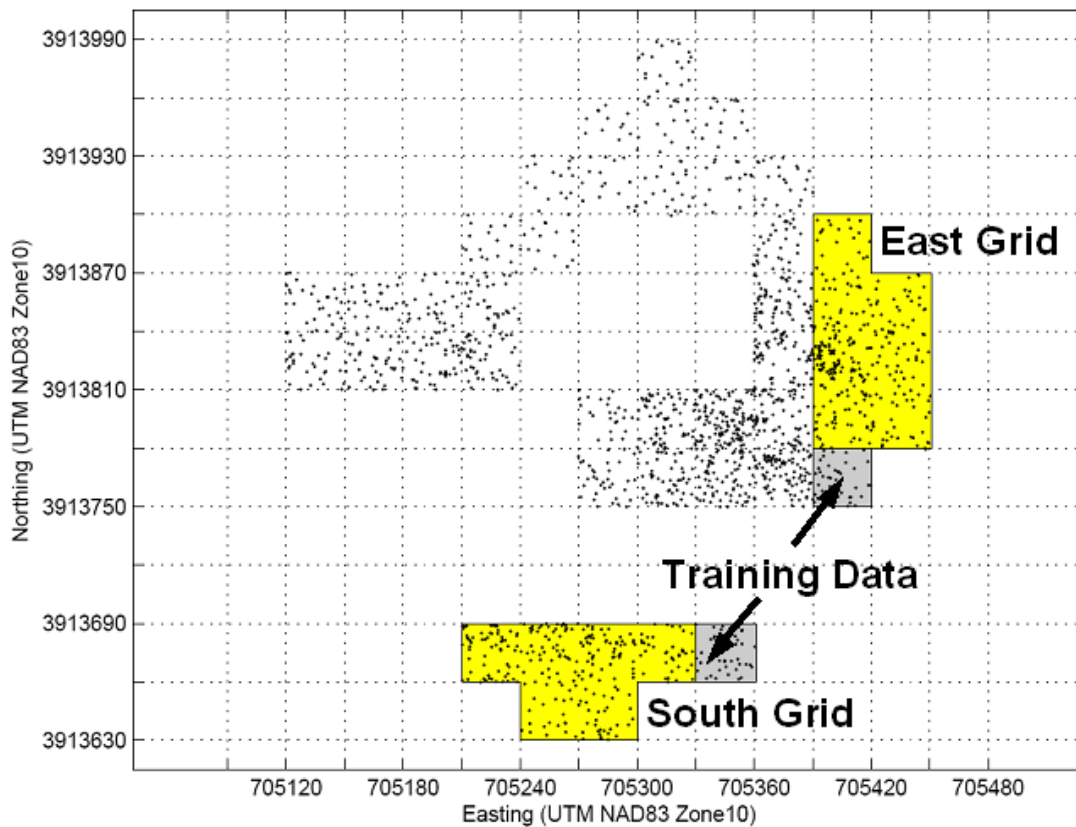

Figure 5: BUD cued survey (in yellow) location. Training data locations are shown in gray.

3.2 Scope of Demonstration

The ESTCP UXO Discrimination Demonstration Site was located at former Camp San Luis Obispo, CA. LBNL performed a discrimination survey of the calibration line, test pit, and targets/locations (flags) provided to us by the ESTCP office.

The calibration line contained four types of UXOs that were expected at the site – 60 mm, 81 mm, and 4.2-in mortars, and 2.35-in rocket. Typical polarizability responses of these objects are shown in Figure 6. Each plot contains major (solid line), medium (dashed line) and minimum (dotted line) polarizabilities as a function of time and a picture of the item.
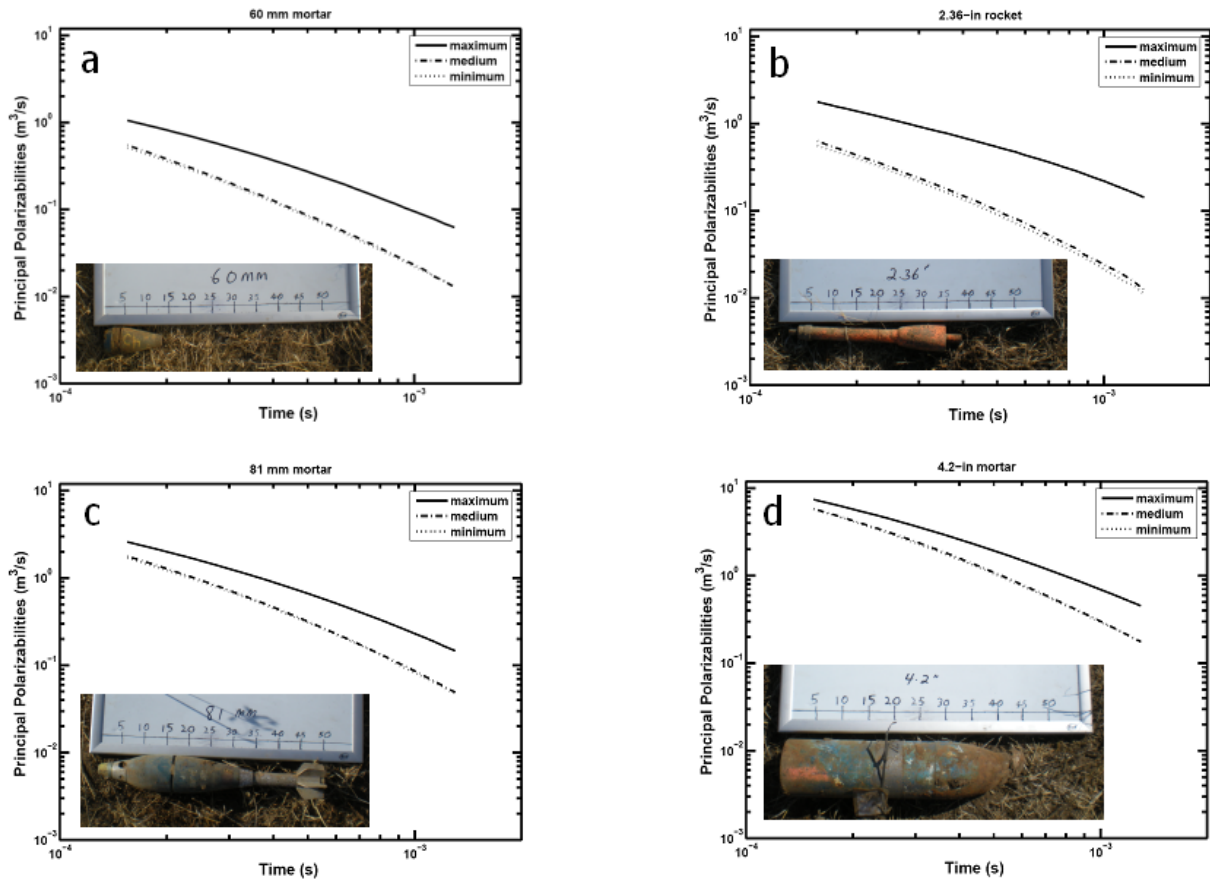

Figure 6: Polarizability responses as a function of time for (a) 60 mm mortar, (b) 2-36 in rocket, (c) 81 mm mortar, and (d) 4.2-in mortar.

The BUD was operated in the cued mode. BUD was brought to marked locations and run in the characterization/discrimination mode. The three discriminating polarizability responses were

recorded and visually presented on the computer screen. The depth and horizontal location with respect to the cart was recorded, together with a GPS location of the reference point on the cart, both corrected for tilt due to a steep terrain, using single object inversion algorithm. As described in Chapter 2.1, object orientation estimates and equivalent dipole polarizability estimates used for large and shallow UXO/scrap discrimination are more problematic as they are affected by higher order (non-dipole) terms induced in objects due to source field gradients along the length of the objects. Therefore, stationary data were collected on 11-point grid around each flag as shown in Figure 7. This allowed the system get further away from the object, and hence minimized source gradients, at one or more locations in the case that a large shallow object was found. The orientation of our short profiles was chosen based on topography, so that we didn't have to push/hold BUD up or down the hill; when possible it was along topography contours. We built a lightweight template that was easy to carry, and the measurements points were painted on the ground with an environmentally friendly paint. BUD then occupied each of the 11 points and acquired a stationary measurement.

The cart was equipped with a two-component tiltmeter and three-component magnetometer. Both devices were calibrated before the survey. The tiltmeters readings were used to compute the cart pitch (positive pitch = cart front down = negative tiltmeter change), and roll (positive=cart rightside down - positive tiltmeter change). The magnetometer values were used to compute vector magnetic field relative to cart coordinates. This was rotated into leveled cart coordinates, using the cart pitch and roll measurements. Knowing the GPS antenna height above the BUD lower cube surface, cart azimuth, tilt, and roll, the offset of the antenna from the cube coordinate origin (at cube bottom center) was calculated and subtracted from the reported GPS coordinates. As an indicator of the accuracy of the computed cart azimuth, the sum of squared differences in horizontal magnitude and vertical components of magnetic field from their average values was computed and normalized by the average squared magnetic field magnitude. Values greater than 2×10^{-4} indicate a likely error in computed orientation greater than 0.8 degrees, and as much as 1 cm mislocation for points at the corners of the 1 m^2 footprint of the device.
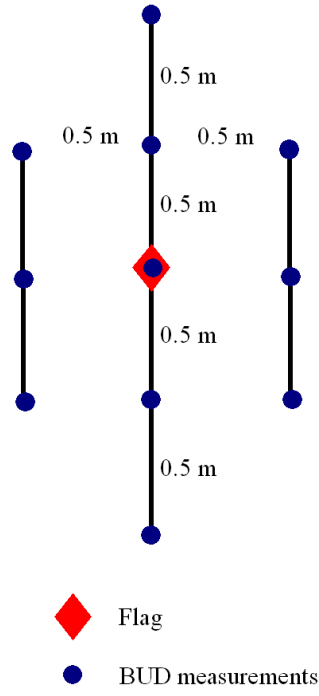
Figure 7: BUD template for 11 measurements around the flag

4. DATA ANALYSIS AND INTERPRETATION

The first step prior to data collection was a system calibration and a background level estimation. We measured the background noise with transmitters in off-position and calculated spectrum of all channels. Then we turned the transmitters on and measured the background field on all channels. This was repeated at least twice to make sure the background field was stable and could be used as the baseline measurement that was subtracted from the data.

Twelve channels of field data were recorded at a rate of 250 k-samples/second for each of three transmitters. Field data were stacked together in a field programmable gate array (FPGA) and transferred to a field computer (laptop) forming a primitive stack, labeled with header information (instrument position, tilt and heading, time stamp, channels of transmitter current, etc). An even number of primitive stacks was averaged together to form stacked data for further processing. The peak transmitter current was estimated from the stacked transmitter current channel record, and the data were normalized by that value. Nominal transmitter shut-off time was estimated, and induction responses were computed at 35 logarithmically spaced times between 140 and 1400 μs, averaged in half-sine windows with widths 10% the center time after transmitter pulse shut-off. Responses were differenced with background responses collected over a nearby site determined to be relatively free of metallic objects by having a system response that varied little with system translation. The resulting 24 channels of normalized responses were then inverted for candidate object position and principal polarizabilities as a function of time after transmitter shut-off. Data before 140 μs were ignored. Polarizability plots for candidate objects were examined for consistency with an inductive object response.

Both field data and inversion results have been archived. The data are retained on a portable external disk, and the inversion results are retained both on the portable external disk and CD-ROM for archiving and distribution.

4.1 UXO/scrap discrimination approach using training data

Characterization of UXO and clutter was done using a training data set that was provided by the ESTCP office (gray area in Figure 5), those collected over the test pit at the site, and data collected over the targets of interest in previous surveys. The training data consisted of sets of principal polarizability responses at 35 logarithmically spaced times centered from 140 μs to 1400 μs after transmitter shut-off. The training data set contained principal polarizability responses of 312 objects - 108 UXO, and 204 pieces of scrap metal. 113 objects were from San Luis Obispo, and 199 from our previous library. The approach in this study was similar to the one applied to the former Camp Sibert data (Gasperikova et al., 2009). However, in this survey, the level of difficulty was increased by presence of multiple objects, and we present a new way how to analyze these kinds of data.

The data time interval was subdivided logarithmically into n_{div} = 3 subintervals. The product of each principal polarizability with its sample time was averaged over each of these intervals. Since there are three principal polarizabilities, this results in n_{feat} = $3n_{div}$ reduced data, henceforth called "features." We used an additional feature, the logarithm of the vector magnitude of the other features (in m^3), which increases the total number of features n_{feat} to $3n_{div}$+1, in this case ten. When this feature was appended, the partial vector of other features was rescaled to have unit magnitude. For each training response or response to be classified, an n_{feat} dimensional vector was constructed from the features of responses. Each of the features had its median and median absolute deviation (MAD) computed separately for UXO and scrap training data.

In cross validation, results from a subset of training data were used to predict something about the remaining training data. This was done many times ("repeats"), excluding a different set of training data each time, and then a choice was made based on what gave the best predictions averaged over many repeats. For the UXO versus scrap discrimination problem, average cross-validated estimated probability of UXO being scrap was 0.052, when the number of subintervals (n_{div}) was 3 (n_{feat} = 10 features) and all training data were used. When only training data from San Luis Obispo were used the average cross-validated estimated probability of UXO being scrap was 0.25. In this work, a constant number of UXO and scrap training data were excluded at

a time, in roughly equal proportions. The number of the excluded data was chosen so that one response was withheld at a time from the smaller of the sets of UXO and scrap training data. The set of excluded data was cycled through excluding each UXO response once and most scrap responses once.

For convenience, features were differenced with median values (for UXO or scrap) and normalized by feature MADs (for UXO or scrap), separately for consideration as UXO or scrap, and denoted by $\mathbf{v}_i^{(uxo)}$ or $\mathbf{v}_i^{(scrap)}$ for the two normalizations, respectively. Training data from UXO and scrap classes were used to form trimmed-feature covariance matrices for the two classes separately:

$$C^{(class)} = \frac{1}{n^{(class)}} \left[\sum_{i \text{ in class}, \left| v_i^{(class)} \right| \le median} v_i^{(class)} (v_i^{(class)})^t + \sum_{i \text{ in class}, \left| v_i^{(class)} \right| > median} median^2 \frac{v_i^{(class)} (v_i^{(class)})^t}{\left| v_i^{(class)} \right|^2} \right] \quad (1)$$

where (class) is either (uxo) or (scrap), t denotes transpose, and $n^{(class)}$ is the number of (class) responses. In the second sum, the contribution of large magnitude feature vectors are downweighted. After forming $C^{(class)}$, it was biased by dividing its off-diagonal elements by $1 + \frac{1}{2}$ $(n^{(class)})^{-1/2}$, damping its smaller eigenvalues. A feature vector $v_i^{(class)}$ probability density function was estimated empirically as

$$f^{(class)}(v_j^{(class)}) = K \sum_{i \text{ in class}} \frac{1}{\left[1 + (v_j^{(class)} - v_i^{(class)})^t (C^{(class)})^{-1} (v_j^{(class)} - v_i^{(class)}) \gamma (n^{(class)})^{2/n_{feat}} \right]^{(n_{feat} + p_{extra}^{(class)})/2}}$$

(2)

with

$$\gamma = 0.2986/(n_{feat} + p_{extra}^{(class)}) \tag{3a}$$

$$K = \frac{1}{2} \left(\frac{\gamma}{\pi} \right)^{n_{feat}/2} \frac{\Gamma((n_{feat} + p_{extra}^{(class)})/2)}{\Gamma(p_{extra}^{(class)}/2)} (\det(C^{(class)}))^{-1/2} \tag{3b}$$

where Γ is the gamma function, and $p_{extra}^{(class)} \ge 2$.

Equation (2) is a generalization of a Cauchy distribution. As $p_{extra}^{(class)}$ approaches infinity the distribution approaches a Gaussian distribution. With parameter $p_{extra}^{(class)} = 3$ the outer exponent has the smallest half-integer value for which distribution has a finite variance. This value allows for very heavy tailed distributions. Empirical probability densities were estimated separately for UXO and scrap classes.

In cross-validation, densities in equation (2) were computed for UXO and scrap classes from non-excluded responses, and feature vectors $v_j^{(uxo)}$ and $v_j^{(scrap)}$ were computed for excluded training responses, where for j'th response, the two differ in component offsets and normalization. The first was used in estimating the response's likelihood as a UXO response, and the second in estimating its likelihood as a scrap response.

Allowing for unequal a priori probability of a response being due to UXO or scrap, with their ratio being α^2, the probability that the response is due to scrap is:

$$p^{(scrap)}(v_j^{(scrap)}) = \frac{f^{(scrap)}(v_j^{(scrap)})}{\alpha^2 f^{(uxo)}(v_j^{(uxo)}) + f^{(scrap)}(v_j^{(scrap)})} \tag{4}$$

(Bayes' rule, e.g., Hoel et al., 1971) and the probability that the response is due to UXO is

$$p^{(uxo)}(v_j^{(uxo)}) = 1 - \frac{f^{(scrap)}(v_j^{(scrap)})}{\alpha^2 f^{(uxo)}(v_j^{(uxo)}) + f^{(scrap)}(v_j^{(scrap)})} \tag{5}$$

Probabilities in Equations (4) or (5) form the basis for the discrimination between UXO and scrap classes. The class feature covariance matrices $C^{(uxo)}$ and $C^{(scrap)}$, and the densities $f^{(uxo)}$ and $f^{(scrap)}$ were computed from subsets of the training data. UXO and scrap probabilities - equations (4) and (5) - were estimated for remaining (excluded) training data. Estimated UXO probabilities of excluded training data were summed over many repeats.

In practice, we choose parameter α^2 empirically. For a given value of α^2, the scrap probabilities of all training data are summed as

$$\left\langle n^{(scrap)} \right\rangle \equiv \sum_j p^{(scrap)}(v_j^{(scrap)}) \tag{6}$$

where the densities entering sum (6) are evaluated as before, excluding the training data for which a density is being calculated from the covariance matrix calculations and the sums in densities in equation (2). Since the number of scrap responses in the training data set is known parameter α^2 is adjusted, so that

$$<n^{(scrap)}> = n^{(scrap)} \tag{7}$$

Quantity (6) is monotonic in α^2, so solution is unique. Newton's method started from $\alpha^2 = 1$, keeping α^2 from decreasing to less than 0.1 of its previous value on any iteration, works very well. Since $p^{(scrap)} = 1\text{-}p^{(UXO)}$, this criterion for setting α^2 also sets the sum of $p^{(UXO)}(v_j^{(UXO)})$ to the number of UXO responses in the training data set.

After computing $f^{(uxo)}(v_j^{(uxo)})$ and $f^{(scrap)}(v_j^{(scrap)})$ for the set of excluded responses, the set of excluded responses was changed, trimmed feature covariance matrices recomputed, and densities computed for the set of new excluded responses. $n_{with}^{(scrap)}$ with unreserved scrap training responses and $n_{cycl} \times n_{with}^{(UXO)}$ with unreserved UXO training responses are cycled through the excluded data sets. Parameter $p_{extra}^{(class)}$ in equation (2) was chosen separately for UXO and scrap classes, in each case using the integer maximizing the log likelihood

$$L^{(class)} \equiv \sum_{j \, in \, class} \log(p^{(class)}(v_j^{(class)})) \tag{8}$$

of the training data of the corresponding class.

In summary, the UXO and scrap data were randomly ordered within the class. A sequence of candidate $p_{extra}^{(class)}$ values were cycled through as an outer loop. Sets of excluded UXO and scrap training data were chosen starting with the first on their randomly ordered lists. Trimmed feature covariance matrices were computed excluding these. Quantities $f^{(uxo)}(v_j^{(uxo)})$ and $f^{(scrap)}(v_j^{(scrap)})$ were computed for the excluded data, and the sum of their logarithms evaluated at the training points accumulated. The sets of excluded responses were changed (moving down the random ordered lists), trimmed feature covariance matrices recomputed, and densities computed for the new set of excluded responses, based on the non-excluded responses. After cycling the training data through the excluded sets, and cycling through the outer loop of prospective $p_{extra}^{(class)}$, $p_{extra}^{(class)}$

was chosen for each of scrap and UXO distributions to maximize the likelihood of the training data.

Once $p_{extra}^{(UXO)}$ and $p_{extra}^{(scrap)}$ was selected, covariance matrices $\mathbf{C}^{(UXO)}$ and $\mathbf{C}^{(scrap)}$ were recomputed using all training data to compute feature medians and MADs for UXO and for scrap responses, and in forming the covariance matrices themselves. Similarly, all training data were then used in reforming empirical distributions for scrap and UXO classes analogously to equations (2) and (3) but summed over all responses, omitting any self-response terms (i = j). The resulting covariance estimates, and empirical probability distributions for $\mathbf{v}^{(scrap)}$ and $\mathbf{v}^{(UXO)}$ were then used to evaluate the probability that a response is due to scrap or UXO through equation (4) using the response's feature vector, shifted and normalized.

After this calibration, the algorithm was applied to the set of unknown responses, and the discrimination between UXO and scrap classes was conducted using equation (4) and (5). Furthermore, the priority dig list was constructed in a following way: (1) each cued location/flag was assigned (2) a probability of being a clutter (least dangerous items first, with a probability equal to one), (3) a rank (integer number starting with 1, and for the category 4 entered -9999), (4) a category (1, 2, 3, or 4 explained below), and (5) overlap status (zero for no overlap, non-zero for overlapping signatures).

The four categories were:

(1) Can Analyze – Likely Clutter

(2) Can Analyze – Can't Decide

(3) Can Analyze – Likely Munition

(4) Cannot Analyze

The cumulative number of anomalies with $p^{(UXO)}$ below a given value is plotted in Figure 8 for TOI (solid) and scrap (dashed) in the SLO training data. Based on the training data, all objects with $p_o^{(uxo)}$ smaller than 0.0005 were considered as clutter. In another words, the boundary between category 1 and 2 was taken at 0.9995 probability of being scrap. The boundary between category 2 and 3 was taken at 0.25 probability of being UXO. Vertical lines in Figure 8 indicate these boundaries.
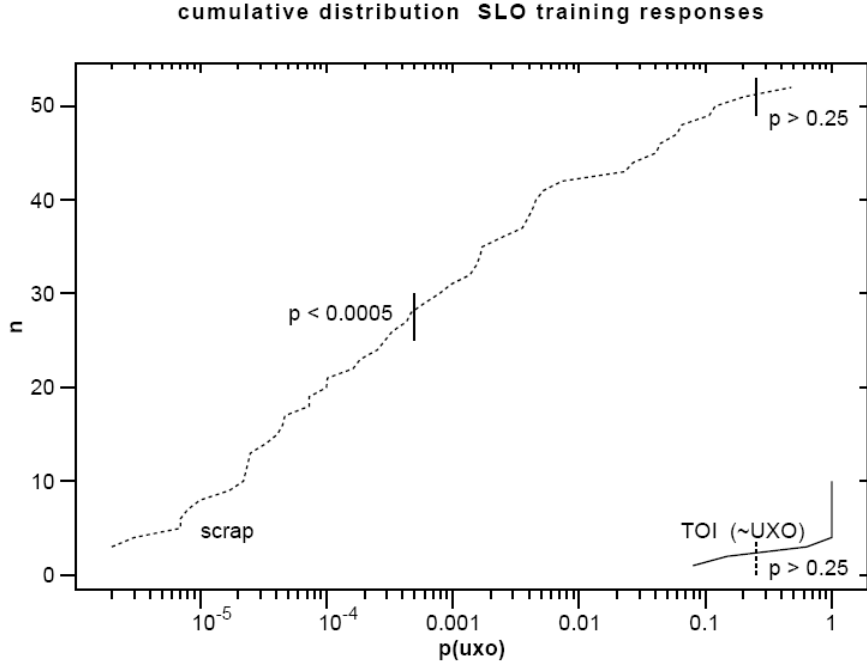
Figure 8: Estimated probabilities of object being scrap or UXO for SLO training data set.

For the purposes of this plot as well as in creating density functions using equation (2), object under flag 1260 was treated as scrap (it has $p^{(UXO)} = 0.000003$]. With these cutoffs there were 28 objects in category 1, 23 in category 2, one in category 3, and three in category 4 for the SLO scrap training data. Similarly, there were zero objects in category 1, one in category 2, and eight in category 3 for the SLO TOI training data. In this training data set analysis we correctly identified 44% of total number of objects that can be left in the ground (scrap), while no TOI was left in the ground. If object 1260 would be considered as TOI, in this analysis, we would have one false negative. Category 4 was defined as (a) measurements at the sites with overlapping signatures (three adjacent anomalies with maxima closer than 3 m), and (b) those which inversions have rms relative residuals greater than 0.5.

Scrap and UXO probability density functions were estimated at the different data point values. Using the maximum of likelihood functions (8) over integer values of $p_{extra}^{(UXO)}$ and $p_{extra}^{(scrap)}$ for the UXO and scrap, probability densities are at $p_{extra}^{(UXO)} = 9$ and $p_{extra}^{(scrap)} = 23$, so these values were

selected. To satisfy criterion that the summed UXO probabilities should yield the true number of UXO in the training set, $\alpha^2 = 15242$ was similarly selected.

4.2 Application of UXO/scrap discrimination approach

In applying the method to data from San Luis Obispo, we allowed for the possibility of multiple objects close to a cued flag. To give sufficient data for distinguishing multiple objects, for each provided location/flag we collected 11 measurements using a scheme shown in Figure 7. Measurements were repeated when GPS accuracy error estimate was greater than 0.02 m. When some sets of measurements were repeated, the set with overall lower GPS error was used, but individual measurements from other sets included when their GPS error was lower. When measurements from several sets were mixed, locations with multiple measurements were weighted approximately inversely with respect to GPS error value. The data were inverted for dipole(s) position and principal polarizability curves as a function of time using the empirical distribution evolutionary algorithm (e.g., Smith and Morrison, 2004, 2005) using multiple site measurements and multiple dipole positions, with dipole positions and polarizabilities as free parameters.

For uncorrelated Gaussian noise, one expects a slight improvement of data fit with increased number of dipoles fitted to the data. For uncorrelated Gaussian noise added to data from objects well approximated by single dipole polarizabilities, one expects larger improvements in data misfit with increased number of dipoles, up to the true number of objects, and slight improvements with additional dipoles. In our case, the data had uncertainties in instrument location between different measurements on the order of 2 cm. Uncertainty in cart position is equivalent to correlated error in the measurements due to differences between what is measured at the actual location, and what would have been measured at the estimated position, and are roughly proportional to the measured data. We approximated this by including an additive 5% relative noise in the data errors used inversely to weight the data (by adding the square of 5% of the data magnitudes to the estimated data variances). Instrument mislocation is correlated between measurements at a single system location, and much less correlated between different system locations used in an inversion.

Because of the presence of instrument location errors, which act as correlated noise, the appropriate cut-off levels of a misfit ratio between one and two dipole inversions, and between two and three dipole inversions was determined from examination of their distributions. The amount of misfit reduction between fitting one- or two-dipoles, and between fitting two- or three-dipoles, for inversions of data sets in the SLO south grid area, is plotted as a scatter plot in Figure 9.
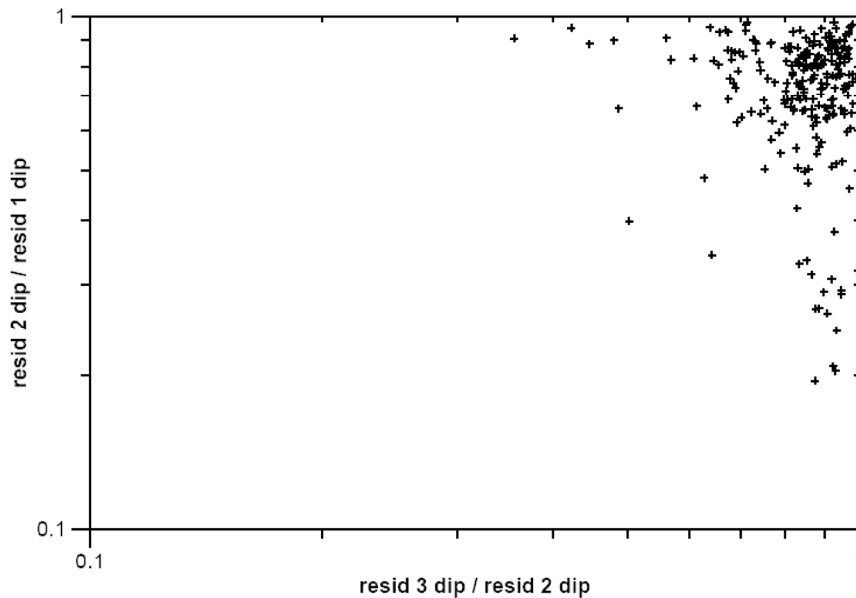

Figure 9: Scatter plot of a misfit between three- and two-dipole inversions and two- and one-dipole inversions.

A small gap in the ratio of three to two-dipole inversion misfits was noted near 0.8 in the scatter plot. A similar small gap in the ratio of two to one-dipole inversion misfits was noted near 0.8. So, 0.8 was used as the separation point for misfit improvements between two and three-dipole inversions; when this misfit ratio was less than 0.8, the data were considered to require a three dipole (three object) interpretation, and when greater than 0.8 a two or one object interpretation.

Data with that ratio greater than 0.8, were similarly divided into two and one object interpretations based on the ratio of misfits of two and one-dipole inversions, with values of this ratio less than 0.8 interpreted with two dipoles, and greater than 0.8 with one dipole. If more than three objects are present, interpretation with the three-dipole model may miss an object. To guard

against this, the rms residual relative to the data at the location closest to the anomaly maximum was considered. Any data with relative residuals greater than 0.5 was considered inadequately fit. Examples of inadequate inversions that would be classified as the category 4 – Cannot Analyze are data from the training data set for flags 1276, 1292, and 1312, which are all scrap responses. Among targets of interest (TOI) in the training data set, six were fitted with one dipole, one with two dipoles, and three with three dipoles. Object under flag 1260 was omitted from the TOI list, because of its asymmetric response. Other scrap training data responses were fitted as follows – 15 with one dipole, 21 with two dipoles and 16 with three dipoles. In training TOI multi-dipole inversions, one object (flag 1253) was split into two dipoles separated 0.24 m with principal polarizabilities displaying symmetry typical of UXO, so both were included as training data. In the three TOI three-dipole inversions, each had one dipole with symmetric principal polarizabilities, which was used as a training response, and the other two dipoles were not used in training or classification. The different dipoles from the multi-dipole scrap inversions were each used as scrap training responses, except three dipoles which were further than 1 m laterally from the nearest sounding and were omitted (one each at flags 759, 858, and 1301). Additionally, anomalies have been classified by the number of adjacent anomalies with maxima closer than 3 m. All the anomalies with more that three adjacent anomalies with maxima closer than 3 m were classified as having overlapping signatures, and as category 4.

Following the process described above, the median normalized time polarizability products for the three binned sample times centered at 0.2135, 0.4341, and 0.9118 ms, for the three principal polarizabilities were (-0.497, -0.438, -0.321), (-0.380, -0.270, -0.150), (-0.355, -0.251, -0.139) for UXO training data, with a median $\log_e$ vector magnitude of 7.12, and were (-0.682, -0.444, -0.198), (-0.369, -0.203, -0.0724), (-0.178, -0.0815, -0.0292) for the scrap training data, with a median $\log_e$ vector magnitude of 3.20, where major principal polarizabilities were grouped together, intermediate principal polarizabilities together, and minor principal polarizabilities together. Thus, the scrap data had magnitudes typically 50 times smaller than the UXO data, had more steeply dipping polarizability curves, and greater separation between major and intermediate principal polarizabilities, and much greater separation between intermediate and minor principal polarizabilities. Median absolute deviations (MADs) and a median $\log_e$ vector magnitude for the UXO were (0.0249, 0.0225, 0.0140), (0.0222, 0.0213, 0.0158), (0.0230,

0.0201, 0.0171), (0.361), and for the scrap data (0.0828, 0.0801, 0.0717), (0.103, 0.0878, 0.0518), (0.106, 0.0585, 0.0245), (0.720). These values illustrate two to five times more variability in scrap responses compared to UXO responses. Medians and MADs for the two classes of data with individual responses removed for computation of densities using equation (2) would be similar, but are too numerous to consider here.

5. PERFORMANCE ASSESMENT

The ground truth at San Luis Obispo contained 59 TOI and 412 pieces of scrap. From the total of 539 cued locations that BUD occupied, 66 were the training data, so the number of flags to be discriminated, using the empirical likelihood ratio approach, was 473, and that was the number of entries in our priority dig list. Items 1-154 were classified as Category 1 - Can Analyze – Likely Clutter and should not be dug, and items 155-473 should be dug. Items 155-281 were classified as Category 2 - Can Analyze: Cannot Decide, items 282-371 were classified as Category3 - Can Analyze: Likely Munition, and items 372-473 were classified as Category 4 - Cannot Analyze. Scoring results from the Institute for Defense Analyses (IDA) are shown in Figure 10. The ROC curve shows relationship between percents of munitions dug and number of unnecessary digs. With 154 items identified as scrap, the TOI that was missed in this analysis was 2.36-in mortar under flag 444. The case of discrimination at the flag 444 is particularly interesting because, in this case, discrimination results depend on whether one-dipole or two-dipole polarizability inversion results were used for the discrimination. For the one-dipole inversion the response was outside of the typical range of values in the UXO training data, and the object was classified as scrap. For the two-dipole inversion, one of the objects was correctly identified as UXO (p^{UXO} =0.84), and the other one was correctly identified as scrap metal.
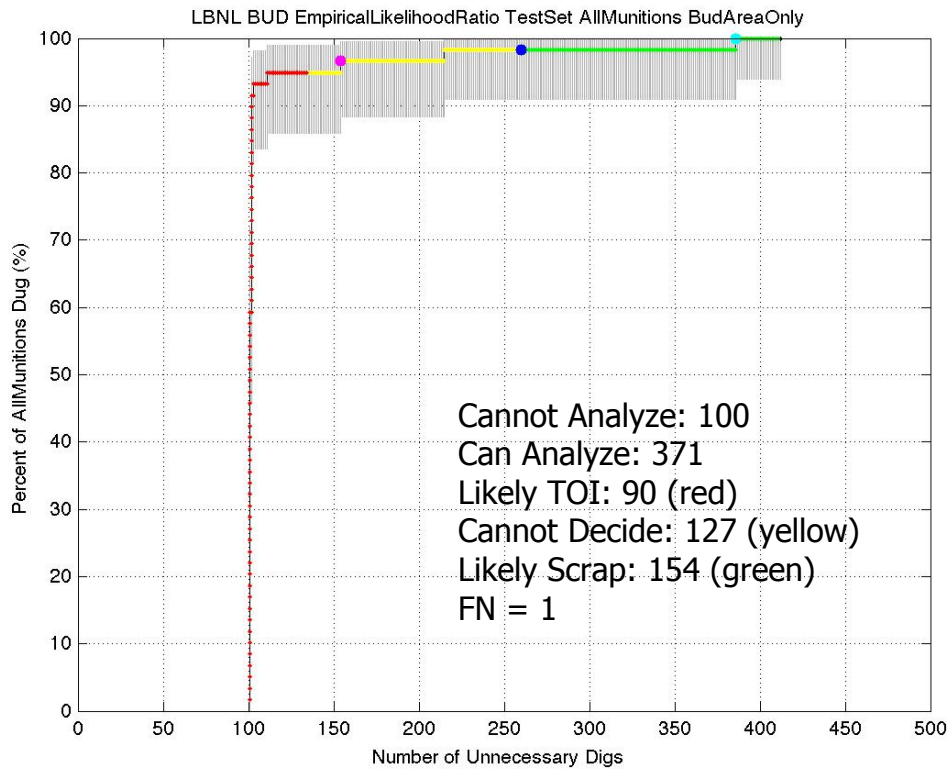
28

Figure 10: ROC curve for the empirical likelihood ratio approach.

In addition to the empirical likelihood ratio approach we submitted also a template match priority dig list. In this approach, polarizability curves were matched with library UXO/scrap responses, and it contained only 'dig'/'nodig' decision for each flag. Since a single object inversion was used to produce these responses, in case it was not clear that only single object is present, if the polarizability response at early times was above 50% of the smallest TOI (60 mm mortar) response, the flag was labeled as 'dig'. Based on this approach items 1- 272 could stay in the ground, and items 273- 473 should be dug. Scoring results from IDA are shown in Figure 11. While it appeared that using this approach we missed 2.36-in mortar under the flag 241/1475, further analysis and discussions showed that this was a surface item, and it was moved during the survey, thus the object was not there when we took the measurements.
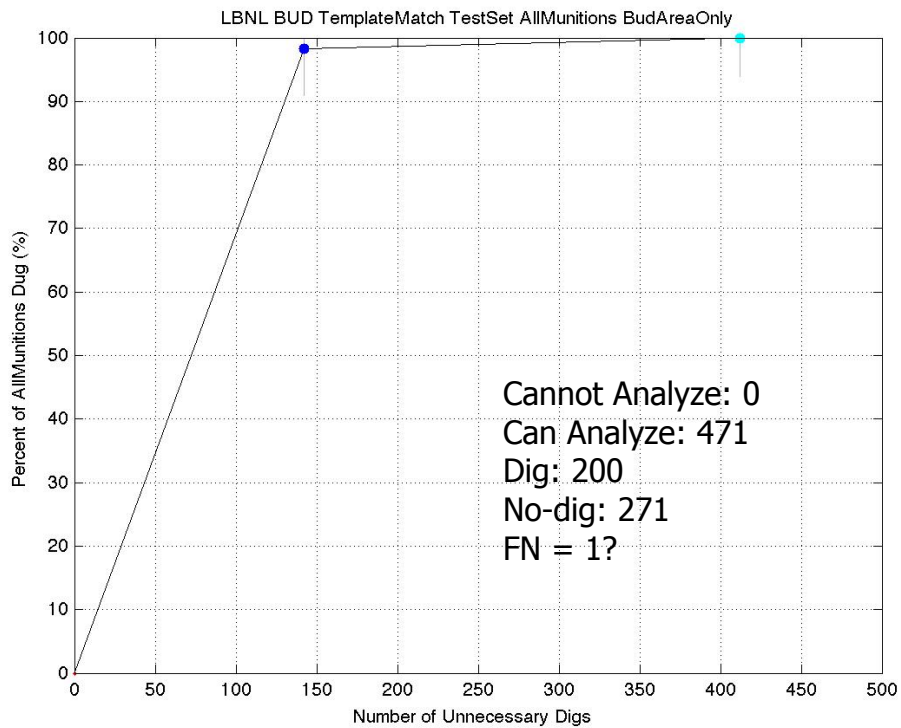
Figure 11: ROC curve for the template match approach.

Using the empirical likelihood ratio approach, ~20% of data were in Cannot Analyze category, 95% of all TOI were correctly identified with only two false positives, while it took ~140 dry holes for the remaining three TOI to be found. The template match approach showed that more than 50% of total number of digs could be saved while correctly identifying all TOI. This approach, however, needs to be automated and produce all supporting statistics before it would be practical to use it in the field.

6. ACKNOWLEDGMENTS

7. REFERENCES

Gasperikova, E., J. T. Smith, H. F. Morrison, A. Becker, and K. Kappler, 2009, UXO detection and identification based on intrinsic target polarizabilities – A case history: Geophysics, **74**, B1-B8.

Hoel, P. G., S. C. Port, and C. J. Stone, 1971, Introduction to Probability Theory: Houghton Mifflin Company.

Smith, J. T., and H. F. Morrison, 2004, Estimating equivalent dipole polarizabilities for the inductive response of isolated conductive bodies: IEEE Transactions on Geoscience and Remote Sensing, **42**, 1208-1214.

Smith, J. T., and H. F. Morrison, 2005, Optimizing receiver configurations for resolution of equivalent dipole polarizabilities in situ: IEEE Transactions on Geoscience and Remote Sensing, **43**, 1490-1498.

Smith, J.T., Morrison, H.F., Doolittle, L.R., and Tseng, H-W., 2007, Multi-transmitter null coupled systems for inductive detection and characterization of metallic objects: Journal of Applied Geophysics, **61**, p. 227–234

8. ACRONYMS

BUD   Berkeley UXO Discriminator

ESTCP   Environmental Security Technology Certification Program

FPGA   Field Programmable Gate Array

GPS   Global Positioning System

IDA   Institute for Defense Analyses

LBNL   Lawrence Berkeley National Laboratory

MAD   Median Absolute Deviations

OSSEPP   Off-Site Safety & Environmental Protection Plan

RTK   Real Time Kinematic

QA/QC   Quality Assurance/Quality Control

SERDP   Strategic Environmental Research and Development Program

TOI   Target of interest

UXO   Unexploded Ordnance

YPG   Yuma Proving Ground